REGULAR PAPER

Advancement of Analytical Model for Hydrophobic Rectangular Pillared Array on Al-Surface and Its Experimental Validation

Sharma Jaishree[1] · Anupam Bhandari[1] · Neha Khatri[2] · Bharpoor Singh[2] · Sahil Jangra[1] · Akmal Husain[1] · Avinash Kumar[3] · M. S. Goyat[1,4]

Abstract

Over the past few decades, self-cleaning surfaces have been significantly investigated due to their commercial applications in various fields. However, the researchers are still lagging in developing better mathematical models and fabricating hydrophobic surfaces for direct espousal in industry. In this study, a force-balanced system-based mathematical model is modified for a rectangular pillared array-based micro-structure and MATLAB simulations were used to validate it theoretically. The same pattern was developed on Al-surface using a single-point diamond turning (SPDT) machine experimentally. The experimental results were validated using coherence correlation interferometry (CCI), optical microscopy, drop shape analyser (DSA), and field emission scanning electron microscopy (FESEM). The experimentally estimated and theoretically predicted contact angles of the rectangular pillared array are found in close agreement. Further, the advancement in mathematical models and models-based surface manufacturing strategies can boost the research in this domain to develop robust self-cleaning hydrophobic surfaces.

Highlights

- A force-balance mathematical model is reformed for a rectangular pillared array structure.
- MATLAB simulations are used to validate it theoretically.
- Rectangular pillared array structure was developed on Al-surface using SPDT.
- The experimental results are validated using CCI, DSA and FESEM.

Abbreviations

θ (°)	The angle between the centre point of the water droplet and the tangential point
l (μm)	Length of rectangular pillars
b (μm)	Width of rectangular pillars
p (μm)	Gap between pillars
rpm	Revolution per minute
rev	Revolution
D	Dimensional
ρ (kg/m^3)	Water density
g (m/s^2)	Acceleration due to gravity
r (mm)	The radius of the circle formed by water droplet
T (N/m)	Water surface tension
H (mm)	Total height of the drop
h (mm)	The distance measured perpendicularly from the drop's centre to its flat bottom contact line
y (mm)	The vertical height of the drop's highest point relative to its horizontal centre
R_0 (mm)	The radius of the spherical drop

✉ M. S. Goyat
goyatmanjeetsingh@gmail.com

1 Department of Applied Science, School of Engineering, University of Petroleum and Energy Studies, Dehradun 248007, India

2 Department of Manufacturing Science and Instrumentation, Central Scientific Instruments Organisation (CSIO), Chandigarh 160030, India

3 School of Computer Science, University of Petroleum and Energy Studies, Dehradun 248007, India

4 Mads Clausen Institute, NanoSYD, University of Southern Denmark, Sonderborg, Denmark

R_1 (mm)	The radius of the drop's projected contact circle with the surface
V (mm)	Drop height
φ	The angle formed by the tangent of the droop and the normal to the rectangular pillar

1 Introduction

The fundamental mechanism of hydrophobic or superhydrophobic surfaces has been the subject of numerous theoretical models in recent years, but it has been difficult to employ any of these models to support an experimental observation for real-world application. As a result of their ability to partially clean themselves, these surfaces have numerous uses in various domains such as anti-fogging [8, 26], anti-corrosion [11, 20–22], anti-icing [17], drag reduction, self-cleaning surfaces [5, 20, 21, 29], etc. Numerous methods for preparing hydrophobic surfaces have been proposed till now. Bottom-up and top-down techniques are frequently used to create micro/nano textured surfaces including laser etching, lithography, electrochemical methods, and so on [7, 9, 14, 16, 31]. The need of generating nanoscale features on metallic or non-metallic surfaces forced the researchers to use highly precise techniques like single-point diamond turning (SPDT). The SPDT machining is the most efficient method [25] for manufacturing technology patterned surfaces with high precision and accuracy. This technique can produce a smooth textured surface with controlled roughness of 2–10 nm [30]. The SPDT can be used for metallic, non-metallic and polymers to design the desired patterns. Aluminium has been selected as the substrate material in the current study due to its low cost, light-weight, high thermal conductivity, and ease of availability [28]. Aluminium is a hydrophilic material, and it has a water contact angle of 85.6°. Aluminium has a wide range of uses, particularly in the biomedical, modern engineering, civilian industries, automobile, aircraft, and transportation [13, 34]. However, in extreme environments, the use of aluminium is constrained by its vulnerability to corrosion and surface contaminations [18]. It is preferable to improve aluminium surface qualities through surface modifications in order to avoid such issues. Creation of a hydrophobic surface on Al is a good alternative to avoid the corrosion of Al. Hydrophobic surfaces are a combination of micro/nano texturing features that support the formation of air pockets between the solid–liquid interface and the water droplet. One of the key elements directly influencing a water droplet's wetting behaviour on a rough surface is surface geometry [1, 15]. The wetting properties are largely caused by two primary factors: the material's low surface energy and surface roughness [3, 6]. As a result, surface characteristics are attributed to a material's intrinsic properties, providing a more accurate interpretation of the structures. This concept is directly related to the wetting theories of the surfaces. Young's equation, which was appropriate for smooth and homogeneous surfaces, first provides the wetting theory [33]. Then, Wenzel's theory came into the picture. It was also effective for homogeneous surfaces but had some roughness components which had certain limitations. Ideally, it is almost impossible to manufacture a single surface that is entirely homogeneous and flawlessly smooth. Hence, there is always some degree of surface roughness exists. To disprove Wenzel's idea, the Cassie-Baxter equation which is only applicable to heterogeneous surfaces with surface roughness factor was introduced. Air pockets may cause the surface to become extremely hydrophobic. Water droplet forms a spherical shape and roll off the surface as a result of the droplet of liquid being unable to pass through the roughness between the cavities. Although it is simple to characterise the states of the classical Cassie-Baxter and Wenzel models for surfaces having ordered roughness, it is frequently challenging to determine the roughness and fractional surface values on such textured surfaces [23]. The fundamental mechanism of these surfaces has been the subject of numerous theoretical models in recent years, but it has been difficult to employ any of these models to support an experimental observation for real-world application [2]. The various geometrical characteristics that can aid in understanding the fundamental ideas behind these surfaces are now being discovered by researchers. The reduction of drag on micro/nano structured surfaces, slip length on hydrophobic surfaces, liquid flow through microchannels, and force balance system on water droplets sitting on the micro/nano structures, and viscosity factors for various liquid flows are all being demonstrated by researchers. Sudeepthi et al. [24] developed a mathematical model to find the irreversible wetting transitions between the Wenzel and Cassie-Baxter state on a nano structured surface. In the Cassie-Baxter state, the liquid sits on top micrometre scale protrusions that originate from the clustering of the nanoparticles. In contrast, the solid portion of the coating is completely covered by the liquid in the Wenzel state, increasing the area fraction [10].

But, till date, the development of hydrophobic surfaces that can last up to a few years is still not achieved due to the lack of understanding of hydrophobic surfaces. Hence, every single parameter is equally important in contributing to the best wetting regime [32]. Although there are several experimental investigations on water-repellent surfaces and similarly many theoretical models available for hydrophobic surfaces. However, very limited studies are available on developing a mathematical model for a hydrophobic surface and replicating that specific surface on a substrate practically. The modification of surface wettability on Al substrates offers significant potential for revolutionizing various industries, including electronics, aerospace, biomedical, and energy sectors. With the increasing demand for advanced

materials with modified surface properties, it is crucial to understand and optimize hydrophobic patterns on Al surfaces to enhance performance and functionality. Achieving hydrophobicity on Al substrates can address challenges related to corrosion resistance [27], water repellency, and adhesion in diverse applications. The ability to modify surface properties through theoretical wetting models allows for the design of materials with improved durability, reduced maintenance costs, and enhanced performance in harsh environments [12]. For real life applications of hydrophobic surfaces, such types of research is imperative. Therefore, a force balanced system based mathematical model is modified for a rectangular pillared array structure and SPDT machining is used to manufacture the same structure on Al to validate the theoretical results. This theoretical model not only enables a systematic understanding of the mechanisms that govern wetting behavior, but also functions as a predictive tool for designing surfaces with desired hydrophobic properties. This theoretical model plays a crucial role in guiding experimental research, providing insights into the complex relationship between surface morphology, chemistry, and environmental factors that influence wetting phenomena.

2 Development of a Mathematical Model

Force balance mathematical model [19] is modified to investigate the hydrophobic character of rectangular pillared array structure. The shape of a water droplet on a surface is influenced by several factors, such as water's surface tension, the material's surface energy, and the interaction between the water and the surface. Textured surfaces, depending on their dimensions and spacing, can affect how a droplet spreads or contracts. The ability of a water droplet to assume a spherical shape on a textured surface depends on the specific properties of the surface texture. If the texture encourages anisotropic wetting and the energy barrier for the droplet to spread along one axis is lower than in other directions, the droplet may take on a more elongated or flattened shape along that axis. Conversely, if the texture is fine and doesn't significantly disrupt the cohesive forces of the water, the droplet may still tend to be roughly spherical, but with modifications due to the texture. The contact angle is typically measured from the solid surface in the direction of the liquid phase. It is the angle between the solid surface and the tangent line to the liquid droplet or meniscus at the three-phase contact point (solid–liquid–air). Pillared textures can influence contact angle and droplet behavior by providing additional surface area and trapping air pockets. Theoretical models often consider the balance of interfacial energies, including the surface energy of the solid and liquid phases.
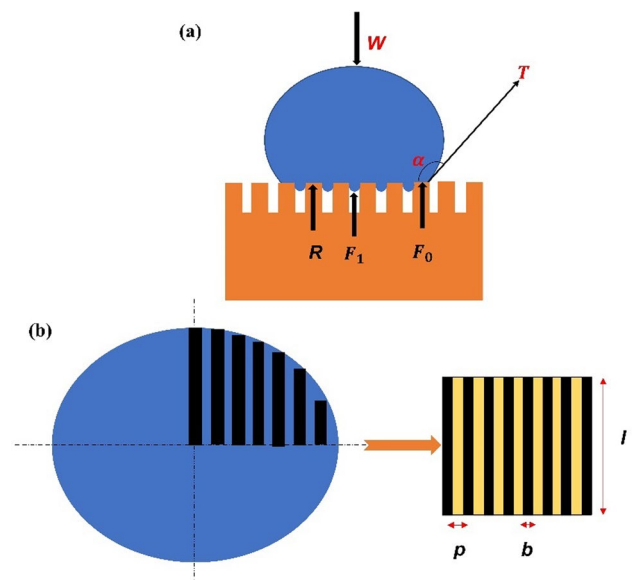

Fig. 1 a Schematics of different forces influencing a water droplet at equilibrium conditions to balance water weight determined by the force balance system; **b** representation of an array of structures with rectangular pillars

Figure 1 depicts several forces operating on a water droplet under equilibrium conditions to balance water weight. The three reaction forces, which are characterized as reaction force by the textured surface, surface tension caused by the drop, and the peripheral surface tension, balance the weight of the water droplet. The relation between the geometrical parameters and water contact angle were determined by evaluating these equations.

Assume that water droplets adhere to the surface. The contact angle is influenced by surface tension and geometrical parameters. Let l be the length of the pillar and b be the width of the geometrical shape pillars. The pillars are assumed to be evenly distributed on the surface. Gravity's influence is ignored along the radial direction. The droplet's radius does not change before or after it lands on the surface. The following force-balance equation can be used to calculate the water droplet's weight:

$$W = R + F_0 + F_1 \tag{1}$$

where W denotes the weight of water drop, R denotes the reaction force by the rectangular pillars, F_0 denotes the surface tension at the periphery and F_1 denotes the surface tension due to water drop.

The following equation is used to determine weight of water droplet:

$$W = \frac{4}{3}\pi R_0^3 \rho g \tag{2}$$

where ρ denotes the density and g denotes the acceleration due gravity.

Reaction forces due to rectangular pillars can be calculated as:

$$R = (h + y)(l.b)\frac{\pi R_1^2 \rho g}{\left(\sqrt{l.b} + p\right)^2}$$ (3)

The water droplet's periphery's surface tension for rectangular pillars is given by:

$$F_0 = 2\pi R_0 cos^2\theta$$ (4)

The line of contact between the water droplet and the pillars tops generates a force called surface tension for rectangular pillars that can be calculated as:

$$F_1 = \frac{4aT\pi R_1^2}{\left(\sqrt{l.b} + p\right)^2}sin\varphi$$ (5)

Using Eqs. (2), (3), (4), and (5), we can reduce the force balance model for the rectangular pillars as:

$$\left(\frac{4}{3}\pi R_0^3\right)\rho g = \left[R_0 sin\theta + R_0 - \frac{1}{12}\left(R_0 cos\theta + \sqrt{l.b} + p\right)\left(R_0 cos\theta + 2\sqrt{l.b} + 2p\right)\right]$$

$$\frac{l.b.\pi R_0^2 cos^2\theta.\rho.g}{\left(\sqrt{l.b} + p\right)^2} + \frac{\pi R_0^2 cos^2\theta}{\left(\sqrt{l.b} + p\right)^2} \times 4\sqrt{l.b}$$

$$\times T sin\left[cos^{-1}\frac{p}{\left[\left(\frac{p}{2}\right)^2 + \left\{\frac{1}{2V}\left[\left(\frac{p}{2}\right)^2 - V^2\right]^2\right\}^{\frac{1}{2}}\right]}\right] + 2\pi R_0 T cos^2\theta$$ (6)

In Eq. (6), θ denote the contact angle, p denote the gap between two rectangular pillars, T denote the surface tension.

Taking the parameter p common from the right side of the above equation, the following expression can be obtained:

$$\left(\frac{4}{3}\pi R_0^3\right)\rho g = \left[R_0 sin\theta + R_0 - \frac{p^2}{12}\left(\frac{R_0 cos\theta}{p} + \frac{\sqrt{l.b}}{p} + 1\right)\left(\frac{R_0 cos\theta}{p} + \frac{2\sqrt{l.b}}{p} + 2\right)\right]$$

$$\frac{l.b.\pi}{p^2}\frac{R_0^2 cos^2\theta}{\left(\frac{\sqrt{l.b}}{p} + 1\right)^2}.\rho g + \frac{\pi R_0^2 cos^2\theta}{p^2\left(\frac{\sqrt{l.b}}{p} + 1\right)^2}.4\sqrt{l.b}.t.sin[cos^{-1}\left\{\frac{p}{2\left[\left(\frac{p}{2}\right)^2 + \left\{\frac{1}{2V}\left[\left(\frac{p}{2}\right)^2 - V^2\right]^2\right\}^{\frac{1}{2}}\right]}\right\}]$$ (7)

$$+ 2\pi R_0 T cos^2\theta$$

For the simplification, assume $\sin\theta = x$, $\cos\theta = \sqrt{(1-x^2)}$, $A = \frac{\sqrt{lb}}{p}$ and $B = \frac{p}{2}$ to obtain the following expression:

$$\frac{4R_0^3 \cdot \rho \cdot g}{3} = \left[R_0 x + R_0 - \frac{p^2}{12} \left(\frac{R_0(1-x^2)}{p^2} + \frac{3(A+1)R_0\sqrt{1-x^2}}{p} + 2(A+1)^2 \right) \right].$$

$$\frac{A^2 R_0^2 (1-x^2)\rho g}{(A+1)^2} + \frac{R_0^2(1-x^2)}{p^2(A+1)^2} \cdot 4\sqrt{l.b}.T\sin\left[\cos^{-1}\left\{ \frac{p}{2\sqrt{(B)^2 + [\frac{1}{2V}\{(B)^2 - V^2\}^2]}} \right\}\right.$$

$$+ 2R_0 T(1-x^2) \tag{8}$$

Now, we can find x from the following expression:

$$x = \left[\frac{4}{3}\frac{(A+1)^2}{A^2(1-x^2)} - 1 + \frac{B^2}{3R_0}\left(\frac{R_0(1-x^2)}{p^2} + \frac{3(A+1)R_0\sqrt{1-x^2}}{p} + \frac{3(A+1)R_0\sqrt{1-x^2}}{p} + 2(A+1)^2 \right) \right]$$

$$- \frac{(A+1)^2}{A^2 R_0}\frac{1}{B^2\rho g}\sqrt{l.b}.T\sin\left[\cos^{-1}\left\{ \frac{B}{\sqrt{(B)^2 + \left[\frac{1}{2V}\{(B)^2 - V^2\}^2\right]}} \right\}\right] - \frac{2T}{R_0\rho g}\cdot\frac{(A+1)^2}{A^2} \tag{9}$$

Finally, we can calculate the contact angle θ as:

$$\theta = \sin^{-1}\left[\frac{4}{3}\frac{(A+1)^2}{A^2(1-x^2)} - 1 + \frac{B^2}{3R_0}\left(\frac{R_0(1-x^2)}{p^2} + \frac{3(A+1)R_0\sqrt{1-x^2}}{p} + \frac{3(A+1)R_0\sqrt{1-x^2}}{p} + 2(A+1)^2 \right) \right.$$

$$\left. - \frac{(A+1)^2}{A^2 R_0}\frac{1}{B^2\rho g}\sqrt{l.b}.T\sin\left[\cos^{-1}\left\{ \frac{B}{\sqrt{(B)^2 + \left[\frac{1}{2V}\{(B)^2 - V^2\}^2\right]}} \right\}\right] - \frac{2T}{R_0\rho g}\cdot\frac{(A+1)^2}{A^2} \right] \tag{10}$$

For calculation of θ, the following values were considered. $a = \sqrt{l.b} = 60 \times 10^{-6}$ m, $R_0 = 0.003$ m, $p = 85 \times 10^{-6}$ m, $g = 9.8$ m/s², $V = 0.001$ m and $\rho = 997$ kg/m³.

The graphical results for the contact angle versus parameter a/p were obtained with the help of MATLAB software.

3 Experimental

The micro-rectangular pillared array surface was created using SPDT machining, one of the well-known production methods that can create sub-micron to nano level structures with great accuracy. Figure 2 represents the schematic view of the fabrication of a rectangular pillared textured surface utilizing SPDT machining. When compared to other micromachining techniques, diamond turning can produce near dimensional tolerances that refers to the allowable deviation from the intended dimensions or specifications of a machined component. It represents the degree of accuracy and precision that can be achieved during the diamond turning process.

3.1 Materials and Specifications

Aluminium (Al) was used as the work piece material in this study to produce micro textured hydrophobic surfaces. Aluminium discs with dimensions of 15 mm in diameter and 3 mm in thickness were used.

3.2 Fabrication of Micro-rectangular Pillared Arrayed Surface on Al

The wedge was entirely removed from the Al work piece on both sides using a diamond tool (Fig. 2a). The mirror-finished surface was prepared for the following stage, which involves fabricating micron-sized rectangular pillared structures (Fig. 2c). After that, the surfaces were cleaned thoroughly in an ultrasonic bath to get rid of any leftover residue or machining chips. The work piece was held in a vacuum chuck to ensure a secure and stress-free grip as well as to stop undesired chips from adhering to the work piece. Table 1 displays the parameters of SPDT machining to develop the desired micro-rectangular pillared arrayed surface on Al. These variables were picked based on those that were utilised in the theoretical modelling. As shown in Fig. 2b, SPDT is utilised to project ordered micro features onto Al. To ensure a good surface finish during the machining process, the work piece was offset such that its face was aligned with the vertical axis. This prevented heat generated at the cutting zone from the machining process from damaging the tool and the work piece. Chlerosol was employed as a coolant. The test was carried out under a constant cooling environment. Under ambient conditions, pillars with a rectangular shape were created on the work piece.

3.3 Characterizations

Coherence Correlation Interferometer (CCI), a white light interferometer (CCI-6000, Taylor Hobson) was used to characterize the surface topographies of the rectangular pillared structures at different magnifications. Field emission scanning electron microscopy (FESEM, Carl Zeiss Germany, model: Zeiss Gemini 300) was utilized to examine the rectangular pillared array structures fabricated on the

Table 1 The parameters of SPDT machining to develop micro-rectangular pillared arrayed surface on Al

| Specifications	Machining parameters
Diamond tool	Single crystal
Nose radius	0.2 mm
Rake angle	0°
Speed of spindle	1000 rpm
Tool feed rate	1 μm/rev
Clearance angle	10°
Depth of cut	5 μm
Pitch of rectangular pillared structure	35.04 μm
Height of rectangular pillared structure	28.84 μm
Width of rectangular pillared structure	47 μm

Al surface. FESEM tests were carried out at an accelerating voltage of 10.0 kV. An optical microscope (Nikon Eclipse MA200) was used to investigate the surface topographies. A contact angle goniometer or drop shape analyser (DSA25, Kruss) was used to determine the water contact angle. The droplet volume was set at 5 μl for all water contact angle measurements and deionized water was used.

4 Results and Discussion

Figure 5 displays optical microscopic pictures of the single scale textured Al surface at various magnifications, including 5X, 10X, and 20X. The surface of Al seems exceptionally smooth with consistent surface roughness due to the diamond turning single texturing (Fig. 3).

Al-sample area of approximately 8×8 mm was scanned using CCI. The CCI was used to extract the 2D cross-sectional profile and 3D topology of the textured surface. Figure 4a–c illustrate the measured 3D and 2D profiles of

Fig. 2 Schematic view of the systematic fabrication of a rectangular pillared textured surface using SPDT machine
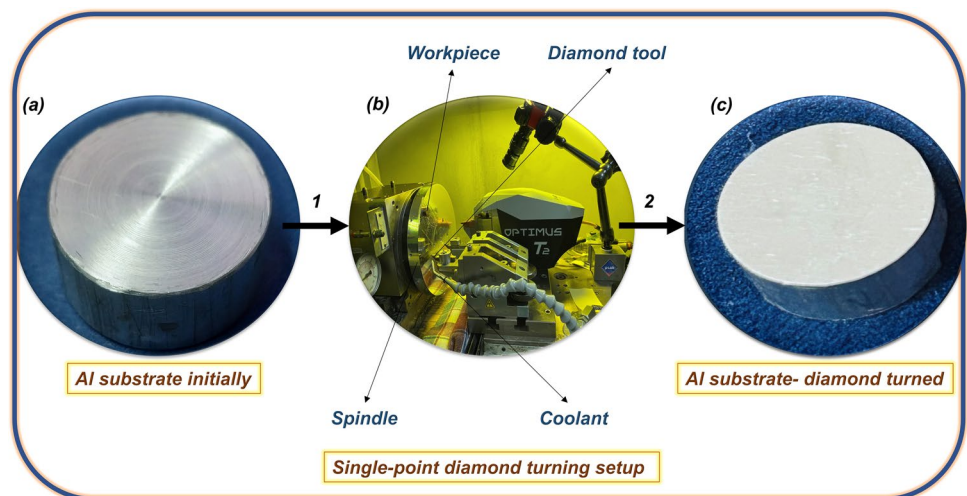
the fabricated rectangular pillars, respectively. Figure 4b depicts the burr formation on rectangular pillars. A burr means rough edges or ridges on a metal. Generally, the burr formation happens during cutting operations on metals. It is common during SPDT machining of metal samples such as Al (in current study). The height (28.84 μm), width (47 μm) and inter-pillar spacing (35.04 μm) of rectangular pillars was measured using a 3D profile of the textured surface.

Figure 5 depicts the FESEM images of rectangular pillared textured surfaces at 200 X, and 1000 X. The individual micro-rectangular pillars on the Al have a slightly tapered shape, which presumably originates from the chip formation during machining. However, the micro-rectangular

pillars are found quite smooth, stable, and periodically patterned, providing the first-level roughness with considerable structural uniformity (Fig. 5a). Even though the surface is thoroughly cleaned in an ultrasonic bath before FESEM characterization, burr formation can be seen at some sites highlighted by dotted circles (Fig. 5b), which may be caused by cutting action during the fabrication process. The burr formation is negligible and can be minimized further by modifying SPDT process parameters. The width (47 μm) and inter-pillar spacing (35.04 μm) of rectangular pillars was further verified using FESEM and found in close agreement with the results of CCI.
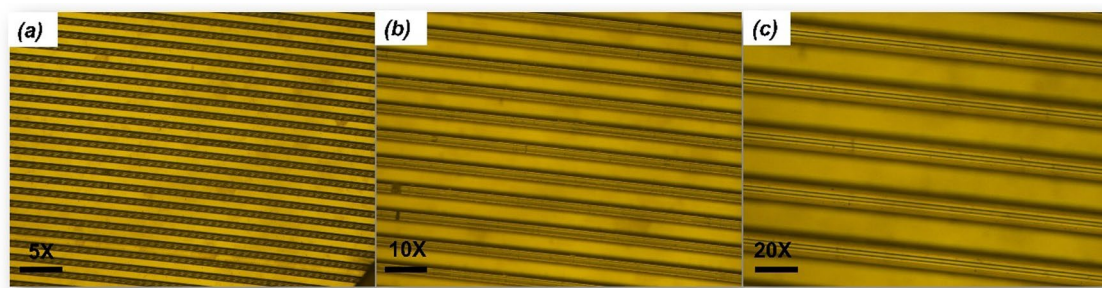

Fig. 3 Illustrations for optical microscopy at various magnifications **a** 5X, **b** 10X, **c** 20X
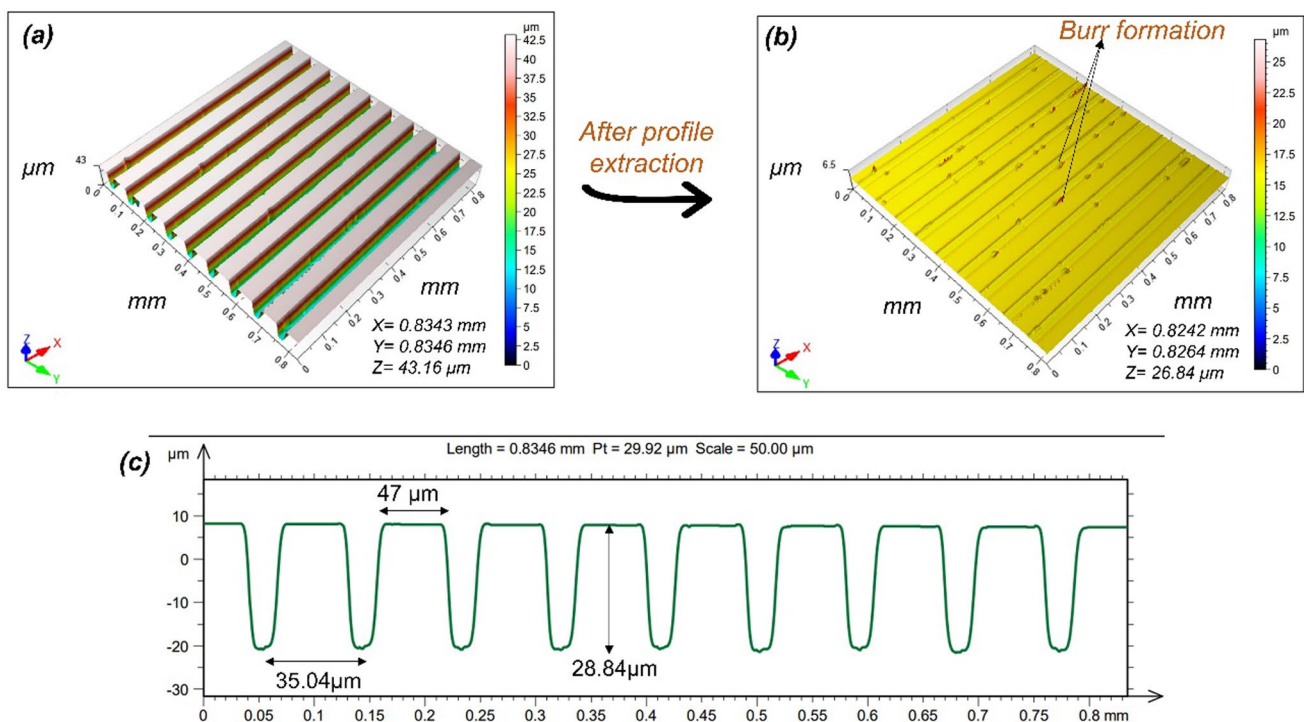

Fig. 4 Identification of surface topographies: **a** Magnified 3-D view of the rectangular pillars, **b** 3-D surface topology after the profile extraction and **c** Extracted 2-D profile of the rectangular pillars

Fig. 5 FESEM images of rectangular pillared textured surfaces at various magnifications **a** 200 μm at 200 X, **b** 10 μm at 1 KX
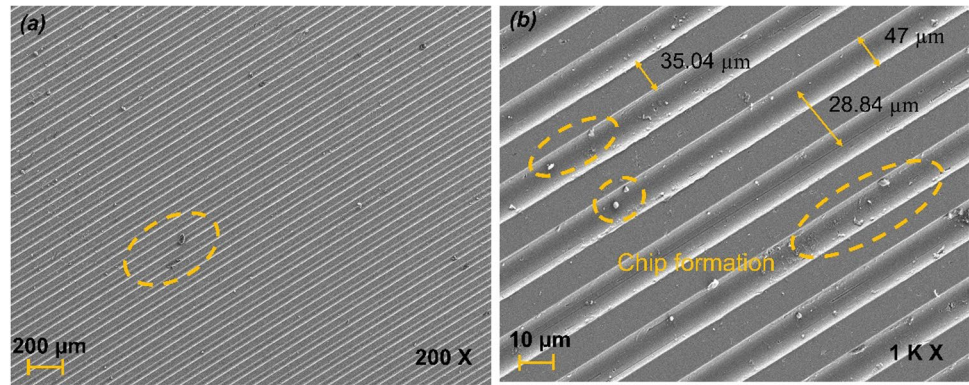

Figure 6a shows the water contact angle of 85.6° on the Al substrate and Fig. 6b shows the water contact angle of 123.7° ± 3° on the particular point of the textured surface. Moreover, Fig. 6c depicts the top view of a water droplet sitting on the textured Al substrate. Figure 6d shows the side view of the water droplet that indicates the water droplet is not immersed inside the rectangular pillars, but it is sitting on the micro protrusions of Al substrate. The low water contact angle on non-textured Al indicates its hydrophilic character; however, the higher contact angle on the textured Al reveals the hydrophobic nature of it. Thus, the wetting regime shifts from hydrophilic to hydrophobic one. The contact angle obtained in Fig. 6b aligns with the theoretical expectations for the Cassie-Baxter regime, which is characterized by reduced wetting. This phenomenon occurs when a liquid droplet sits on a rough or patterned surface, and instead of completely wetting the surface, it partially traps air pockets between the liquid and solid interface. The result indicates that the observed patterned surface represents areas where the Cassie-Baxter wetting state predominates, as higher contact angles are indicative of reduced wetting. Therefore, this study supports the contact angle model that strengthens the theoretical basis for the application of hydrophobic patterns on Al substrates. As a result, the single scale texturing has produced the hydrophobic properties of

the textured Al. Furthermore, adding double texturing to the substrate can improve contact angle and it can even lead to the formation of a superhydrophobic surface [4].

5 Difference Between Theoretical and Experimental Findings

Generally, the scaling factor (a/p = 1) gives the maximum water contact angle for the desired size to spacing factor. This implies that maintaining a balanced relationship between substrate size and spacing can optimize the hydrophobic properties of the surface. In the existing work, the scaling ratio (a/p = 1) for the rectangular pillared structures is considered. The Roy et al. [19] model with a square pillared textured surface provided the initial validation of the mathematical model. An experiment using a single textured surface with single point diamond turning machining at (l = 47 μm and p = 35.04 μm) revealed an average CA of 123.7° ± 3° of the textured surfaces, somewhat near to the projected value of 136.6°. The difference between the experimental results and the value predicted by the theoretical model anticipated is 9.4%. Here, aspect ratio is the reason. Our aspect ratio for the experimental work was close to 1.48, and it has been demonstrated in the literature that an aspect ratio of 1.0 can result
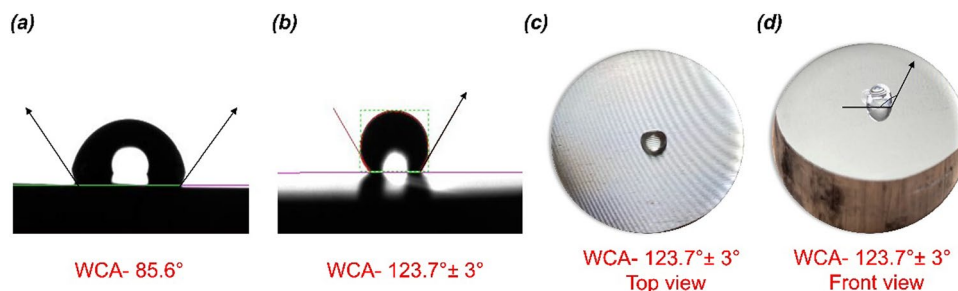

Fig. 6 A visual representation of the contact angle with the water: **a** water contact angle (85.6°) on bare aluminium **b** employing a drop shape analyser to determine the water contact angle (123.7° ± 3°) on textured aluminium, **c** water droplet sitting on a single textured surface, **d** illustration of the water contact angle at 123.7° ± 3° on a particular one point of the textured surface

Fig. 7 For the simulated results, a graphical representation of water contact angle and aspect ratio **a** for 'a' is fixed and 'p' tends to fluctuate; **b** for 'p' is fixed and 'a' tends to vary; and **c** a graphical display highlighting the discrepancy between theoretical and experimental results
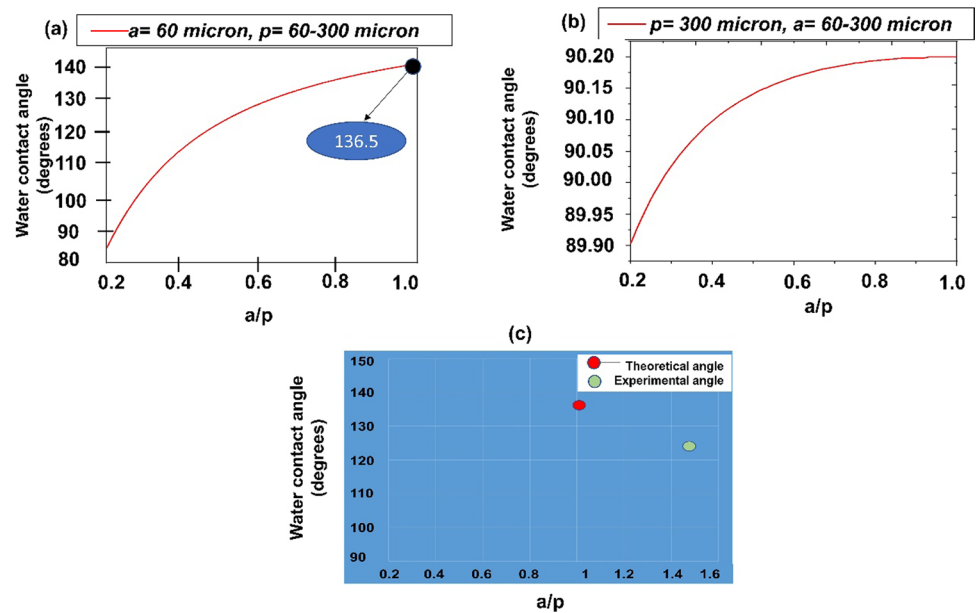
in the highest water contact angle. The single-level textured surface is another factor. Because the maximum contact angle is provided by a combination of micro and nano texturing structures. This demonstrates the differences between theoretical and experimental results. Figure 7a depicts a graphical representation of water contact angle and aspect ratio for different values of 'p' while 'a' is fixed. Figure 7b depicts a graph for different values of 'a' while 'p' is fixed. Figure 7c represents a graph highlighting the difference between the theoretical and experimental results.

The machining parameters have a significant impact on the difference between experimental and theoretical findings. The lowering in the water contact angle is caused by the presence of burr formation in conjunction with the rectangular pillared array. In a rectangular pillared array with three-dimensional high-frequency vibrating modes, the water droplet expands in the feed direction, which reduces the wettability performance of the textured surface and causes the variation. Moreover, the tool feed rate is a significant aspect, since it influences the radius of the machined groove profile, which decreases as the feed rate is increased. The rise in feed rate causes the increase in cutting force, which in turn causes a burr effect on the textured surface.

An additional important factor that leads to discrepancies is precipitates [30]. If the stress value does not exceed the stress limit, the precipitates may be pushed by the diamond tool and move in the direction of the cutting. In this situation, the machined surface develops deeper pits and scratch marks. The surface of the precipitate becomes cracked and uneven when it is manipulated with a diamond tool, which further reduces the water contact angle. A thorough analysis that focuses on fabricating complex structures using SPDT machining is required. Directly creating nanostructures on

the substrate's surface via SPDT machining is difficult. To fulfil the wetting regime, tool optimisation is required since depth of cut and tool feed rate are crucial factors. Geometrical characteristics, such as the width, pitch, and height of the structures, are crucial in self-cleaning applications since they are related to the water contact angle.

6 Conclusions

Force balanced system based mathematical model is modified for rectangular pillared array based micro-structure to anticipate the relationship between the water contact angle and other geometrical parameters that influence the wettability conditions. The theoretical model suggested a water contact angle of 136.6° whereas, the average experimental water contact angle of 123.7° ± 3° was achieved on the textured Al substrate. Compared to hydrophilic non-textured Al, the textured Al exhibited the hydrophobic character. The variation in theoretical and experimental water contact angles of textured Al surface are caused by machining issues like depth of cut, tool feed rate and other factors. Such type of research can motivate the researchers towards better understanding of the scientific principles behind the wetting mechanisms of textured surfaces, which are imperative to develop economical, real-world self-cleaning materials.

Availability of data materials Raw data of the research article is available with the authors and will be provided as per the request from the journal.

Declarations

Competing interest The authors certify that none of their known financial conflicts of interest or close personal ties might have appeared to have influenced the research presented in this study.

References

1. Cheng, C. T., Zhang, G., & To, S. (2016). Wetting characteristics of bare micro-patterned cyclic olefin copolymer surfaces fabricated by ultra-precision raster milling. *RSC Advances, 6*(2), 1562–1570. https://doi.org/10.1039/c5ra20809b

2. Dwivedi, S., Dixit, A. R., Das, A. K., & Nag, A. (2023). A novel additive texturing of stainless steel 316L through binder jetting additive manufacturing. *International Journal of Precision Engineering and Manufacturing-Green Technology, 4*, 1–9.

3. Evans, R., Stewart, M. C., & Wilding, N. B. (2019). A unified description of hydrophilic and superhydrophobic surfaces in terms of the wetting and drying transitions of liquids. *Proceedings of the National Academy of Sciences of the United States of America, 116*(48), 23901–23908. https://doi.org/10.1073/pnas.1913587116

4. Feng, J., Tuominen, M. T., & Rothstein, J. P. (2011). Hierarchical superhydrophobic surfaces fabricated by dual-scale electron-beam-lithography with well-ordered secondary nanostructures. *Advanced Functional Materials, 21*(19), 3715–3722. https://doi.org/10.1002/adfm.201100665

5. Hooda, A., Goyat, M. S., Kumar, A., & Gupta, R. (2018). A facile approach to develop modified nano-silica embedded polystyrene based transparent superhydrophobic coating. *Materials Letters, 233*, 340–343. https://doi.org/10.1016/j.matlet.2018.09.043

6. Hooda, A., Kumar, A., Goyat, M. S., & Gupta, R. (2022). Estimation of surface roughness for transparent superhydrophobic coating through image processing and machine learning. *Molecular Crystals and Liquid Crystals, 726*(1), 90–104. https://doi.org/10.1080/15421406.2021.1935162

7. Jaishree, Bhandari, A., Khatri, N., Mishra, Y. K., & Goyat, M. S. (2023). Superhydrophobic coatings by the hot embossing approach: Recent developments and state-of-art applications. *Materials Today Chemistry, 30*, 101553. https://doi.org/10.1016/j.mtchem.2023.101553

8. Jeon, Y., Nagappan, S., Li, X., Lee, J., Shi, L., Yuan, S., Lee, W., & Ha, C. (2021). *Highly transparent, robust hydrophobic, and amphiphilic organic—Inorganic hybrid coatings for antifogging and antibacterial applications.* https://doi.org/10.1021/acsami.0c20401

9. Jerin, W. R., Je, S., Seung, P., & Moon, K. (2023). A design optimization framework for 3D printed lattice structures. *International Journal of Precision Engineering and Manufacturing, 1*, 145–156.

10. Kang, Y., Jang, G., Kim, G. E., Kwon, S., Lee, M. G., & Jeon, Y. (2022). Design of high-durability superhydrophobic microsurface structures. *International Journal of Precision Engineering and Manufacturing, 23*(8), 929–942.

11. Kim, M., Kim, Y., & Han, S. (2022). Mechanical reliability prediction of foldable displays using subcritical crack growth in siloxane-based cover window by two-point bending test. *International Journal of Precision Engineering and Manufacturing, 23*(11), 1301–1313.

12. Kim, T., Yun, T. H., Yim, C., & Kim, J. (2023). Fabrication of short circuit-preventing electrodes with a self-assembled monolayer on flashlight-sintered porous copper nanofilms. *International Journal of Precision Engineering and Manufacturing, 24*(1), 43–52.

13. Laghari, R. A., He, N., Jamil, M., Hussain, M. I., Gupta, M. K., & Krolczyk, G. M. (2023). A state-of-the-art review on recently developed sustainable and green cooling/lubrication technologies in machining metal matrix composites (MMCs). *International Journal of Precision Engineering and Manufacturing-Green Technology, 9*, 1–24.

14. Lee, J., Chua, P. C., Chen, L., Ng, P. H. N., Kim, Y., Wu, Q., Jeon, S., Jung, J., Chang, S., & Moon, S. K. (2023). Key enabling technologies for smart factory in automotive industry: Status and applications. *International Journal of Precision Engineering and Manufacturing, 1*(1), 94–105.

15. Mittal, A., Verma, S., Iqbal, S. M., Gupta, R., Goyat, M. S., Kaur, K., & Nippani, S. K. (2018). A short review on challenges in fabrication of oil repellent surfaces. *International Journal of Research and Analytical Reviews (IJRAR), 862*(04), 862–866.

16. Paven, M., Mammen, L., & Vollmer, D. (2016). Challenges and opportunities of superhydrophobic/superamphiphobic coatings in real applications. In *RSC smart materials* (Vol. 2016-Janua, Issue 20). https://doi.org/10.1039/9781782622192-00209

17. Rajiv, S., Kumaran, S., & Sathish, M. (2019). Long-term-durable anti-icing superhydrophobic composite coatings. *Journal of Applied Polymer Science, 136*(7), 1–6. https://doi.org/10.1002/app.47059

18. Rodič, P., Kapun, B., & Milošev, I. (2022). Superhydrophobic aluminium surface to enhance corrosion resistance and obtain self-cleaning and anti-icing ability. *Molecules.* https://doi.org/10.3390/molecules27031099

19. Roy, T., Sabharwal, T. P., Kumar, M., Ranjan, P., & Balasubramaniam, R. (2020). Mathematical modelling of superhydrophobic surfaces for determining the correlation between water contact angle and geometrical parameters. *Precision Engineering, 61*, 55–64. https://doi.org/10.1016/j.precisioneng.2019.10.005

20. Sharma, K., Hooda, A., Goyat, M. S., Rai, R., & Mittal, A. (2022). A review on challenges, recent progress and applications of silica nanoparticles based superhydrophobic coatings. *Ceramics International, 48*(5), 5922–5938. https://doi.org/10.1016/j.ceramint.2021.11.239

21. Sharma, K., Malik, M. K., Hooda, A., Pandey, K., Sharma, J., & Goyat, M. S. (2022). Triethoxyoctylsilane-modified SiO_2 nanoparticle-based superhydrophobic coating for corrosion resistance of mild steel. *Journal of Materials Engineering and Performance.* https://doi.org/10.1007/s11665-022-07580-z

22. Sharma, V., Sharma, V., Goyat, M. S., Hooda, A., Pandey, J. K., Kumar, A., Gupta, R., Kumar, A., Prakash, R., & Baptist, J. (2020). Progress in organic coatings recent progress in nano-oxides and CNTs based corrosion resistant superhydrophobic

coatings: A critical review. *Progress in Organic Coatings, 140,* 105512. https://doi.org/10.1016/j.porgcoat.2019.105512

23. Starinskiy, S. V., Bulgakov, A. V., Gatapova, E. Y., Shukhov, Y. G., Sulyaeva, V. S., Timoshenko, N. I., & Safonov, A. I. (2018). Transition from superhydrophilic to superhydrophobic of silicon wafer by a combination of laser treatment and fluoropolymer deposition. *Journal of Physics D: Applied Physics.* https://doi.org/10.1088/1361-6463/aac641

24. Sudeepthi, A., Yeo, L., & Sen, A. K. (2020). Cassie–Wenzel wetting transition on nanostructured superhydrophobic surfaces induced by surface acoustic waves. *Applied Physics Letters, 116*(9), 1–6. https://doi.org/10.1063/1.5145282

25. Sujuan, W., Hao, S., Haojie, M., Feng, X., & Ziqiang, Y. (2019). Characterization of the material-induced elastic–plastic deformations in ultra-precision diamond cutting. *Journal of the Brazilian Society of Mechanical Sciences and Engineering, 41*(9), 1–10. https://doi.org/10.1007/s40430-019-1872-y

26. Türk, S. (2022). Characterization of chitosan/polyethylenimine film layer as a novel anti-fog coating surface. *Journal of Applied Polymer Science.* https://doi.org/10.1002/app.52884

27. Vazirinasab, E., Jafari, R., & Momen, G. (2018). Application of superhydrophobic coatings as a corrosion barrier: A review. *Surface and Coatings Technology, 341,* 40–56. https://doi.org/10.1016/j.surfcoat.2017.11.053

28. Wan, Y., Liu, Z., Lian, Z., Yu, H., & Xia, K. (2015). *The improvement of the aluminum alloy 6061 surface hydrophobic property by using wire cut electrical discharge machining* (pp. 677–681). Aemt. https://doi.org/10.2991/icaemt-15.2015.129

29. Wang, P., Wang, H., Li, J., Ni, L., Wang, L., & Xie, J. (2021). A superhydrophobic film of photovoltaic modules and self-cleaning performance. *Solar Energy, 226,* 92–99. https://doi.org/10.1016/j.solener.2021.08.018

30. Wang, S., Xia, S., Wang, H., Yin, Z., & Sun, Z. (2020). Prediction of surface roughness in diamond turning of Al6061 with precipitation effect. *Journal of Manufacturing Processes, 60,* 292–298. https://doi.org/10.1016/j.jmapro.2020.10.070

31. Yamamuro, Y., Shimoyama, T., & Yan, J. (2022). Microscale surface patterning of zirconia by femtosecond pulsed laser irradiation. *International Journal of Precision Engineering and Manufacturing-Green Technology, 9*(2), 619–632.

32. Yu, D. I., Kwak, H. J., Park, C., Choi, C., Sapkal, N. P., Hong, J., & Kim, M. H. (2019). Wetting criteria of intrinsic contact angle to distinguish between hydrophilic and hydrophobic micro-/nano-textured surfaces: Experimental and theoretical analysis with synchrotron X-ray imaging. *Langmuir, 35*(10), 3607–3614. https://doi.org/10.1021/acs.langmuir.8b03407

33. Zaman Khan, M., Militky, J., Petru, M., Tomková, B., Ali, A., Tören, E., & Perveen, S. (2022). Recent advances in superhydrophobic surfaces for practical applications: A review. *European Polymer Journal.* https://doi.org/10.1016/j.eurpolymj.2022.111481

34. Zheng, S., Li, C., Fu, Q., Li, M., Hu, W., Wang, Q., Du, M., Liu, X., & Chen, Z. (2015). Fabrication of self-cleaning superhydrophobic surface on aluminum alloys with excellent corrosion resistance. In *Surface and coatings technology* (Vol. 276). Elsevier. https://doi.org/10.1016/j.surfcoat.2015.07.002
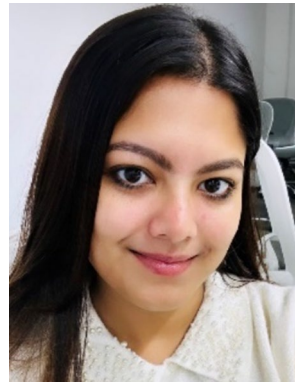
Sharma Jaishree works as a research fellow at the University of Petroleum and Energy Studies (UPES) in Dehradun, Uttarakhand, India. Her research interests include the fabrication of superhydrophobic surfaces for self-cleaning solar panel applications, as well as mathematical modelling on superhydrophobic surfaces. 2020; Panjab University, Chandigarh, India. (Master of Science in Physics), 2018; CDLU, Haryana, India. (Bachelor of Science, Non-Medical).

Dr. Anupam Bhandari is an Associate Professor of Mathematics with UPES Dehradun India. His research interest is ferrofluids, fluid dynamics and mathematical modelling; 2014 NIT Kurukshetra (Ph.D.-Mathematics).

Dr. Neha Khatri is a Principal Scientist at Department of Manufacturing Science & Instrumentation, CSIR-Central Scientific Instruments Organisation, Chandigarh. She received her Ph.D. in Opto-mechanical instrumentation and M.Tech in Advanced Instrumentation Engineering from AcSIR, CSIR-CSIO. Her field of specialisation is Optical system Design and fabrication for X-Rays, Infrared Optical elements, Simulation based modeling, Ultra precision machining of optics for improving the figure and finish accuracy in nanometric range. She has a research experience of more than 11 years in the field of ultra-precision machining for various projects of societal and strategic importance. Her research findings and investigations have received recognition through high impact publications, international collaborations, as well as transfer of technologies.

Mr. Bharpoor Singh a mechanical engineer, currently holds the position of Project Fellow at CSIR-CSIO, Chandigarh. His primary research focuses on the advancement and optimization of ultra-precision machining methods, with a particular emphasis on single-point diamond turning, alongside metrology applications. He has four years of experience in the fabrication of ultra-precise optics, including lenses, mirrors, diffractives, torics, and freeform surfaces. He obtained his B.Tech degree from Punjab Technical University in 2018.

Mr. Sahil Jangra is presently pursuing his PhD degree from University of Petroleum and Energy Studies (UPES), Dehradun, India. His research interests in 2D materials, MXene, Metal oxides, Supercapacitors and Water Purification; 2022 Guru Jambheshwar University of Science and Technology, India (Dual Degree B.Sc. (Hons.) Physics-M.Sc. Physics).

Dr. Akmal Husain received his doctorate (Ph.D.) from the Indian Institute of Technology, Banaras Hindu University, Varanasi. The field of gas dynamics involving non-linear wave propagation phenomena is his primary area of research competence. The work of Dr. Husain encompasses a wide range of areas, including partial differential equations with quasilinear systems, analytical and numerical solutions to nonlinear wave problems in gas dynamics, conservation laws with hyperbolic systems, and partial differential equations with Lie group analysis. He is now dedicated to solving gas-dynamic flow issues using mathematical and numerical methods for hyperbolic partial differential equations.

Dr. Avinash Kumar was working with the University of Petroleum Studies (UPES), Dehradun while working on this manuscript. His research interests include dynamical systems, control design, optimal control theory, and convex optimization. He did his Ph.D. from the Indian Institute of Technology, Mandi in 2022.

Dr. Manjeet Singh Goyat is a Visiting Researcher at University of Southern Denmark. He is Sr. Associate Professor at University of Petroleum and Energy Studies (UPES) in Dehradun, India. His research is primarily focused on the development and characterization of polymer matrix nanocomposites, hybrid polymer nanocomposites, nanomaterial synthesis, functionalization, and superhydrophobic coatings for self-cleaning and anti-corrosion applications. He earned his Ph.D. in Materials Engineering from the Indian Institute of Technology, Roorkee, India. He has made significant contributions to the scientific community and published numerous research papers in renowned journals. He served as a Guest Editor for the reputed journals and as a reviewer for international research grants. He has been the recipient of prestigious government-funded research grants.